

# COMPOSITE MATERIAL PROPERTIES CHARACTERIZATION USING DIGITAL IMAGE CORRELATION AND FINITE ELEMENT MODEL UPDATING: UNCERTAINTY ANALYSIS

He TiRen<sup>1</sup>, Liu Liu<sup>1</sup> and Makeev Andrew<sup>2</sup>

<sup>1</sup> School of Aerospace Engineering, Beijing Institute of Technology, Beijing, China, 100083.  
liuliu@bit.edu.cn

<sup>2</sup> Department of Mechanical and Aerospace Engineering, University of Texas at Arlington, Arlington,  
Texas. makeev@uta.edu, <http://www.uta.edu/mae/AMSL/>

**Keywords:** Global finite-element based approximation, Uncertainty, Digital Image Correlation  
Identification, Finite-element-model-updating

## ABSTRACT

This work presents an uncertainty analysis of displacement measurement, strain assessment due to intrinsic measurement error in digital image correlation (DIC) technique and reconstruction approximation approach. The effect of such uncertainty on the extracted material properties has been illustrated by a modified short beam shear (SBS) test. The noisy and discrete displacement field has been measured by DIC, and displacement and strain fields are constructed using a global finite-element based approximation method. Using a linear least-squares regression method and finite-element-model updating (FEMU), multiple composite material constants were extracted from the FEM-calculated stress and DIC-reconstructed strain field simultaneously. A key observation was the presence of Gaussian distributed measurement error and approximation reconstruction error in reconstructing displacement field and strain field, which must be tracked along the identification procedure to provide uncertainties for the extracted material constants. The effects of the measurement error in DIC and reconstruction parameter on the uncertainty of the extracted material properties have been investigated. The identified results from the area of interest and the full-field area have been compared. The effect of the number of images on the identified material constants has been discussed. The results demonstrate that the standard deviation of the material constant depends on the size of the displacement field and the number of images used in the identification procedure. It increases linearly with the standard deviation of the Gaussian distributed measurement error and decreases nonlinearly with increasing the reconstruction mesh size. Reconstruction mesh size is a crucial parameter and no material constants can be extracted from the identification procedure reliably as it deviates from an optimal value significantly.

## 1 INTRODUCTION

Composite materials with highly-anisotropic mechanical properties are becoming more crucial in advanced structural designs. Growing worldwide demand has resulted in the rapid development of a wide range of composite materials, including glass- and carbon-reinforced polymer-matrix composites. However, the lack of accurate material properties required for a detailed understanding of deformation and failure mechanisms has caused significant delays in the qualification of composite materials for structural applications, and results in extremely conservative design methodologies. Improved three dimensional stress-strain constitutive relations are needed to more accurately characterize the mechanical response of advanced composites.

To enable a cost-effective measurement of three-dimensional constitutive properties of composite materials, including nonlinear stress-strain relations, it is desirable to have a simple, yet effective method that can be used to extract multiple mechanical properties in constitutive relationships from a single test. Full-field displacement measurement techniques can be used to acquire displacements and strains over the entire surface of a specimen. Complex strain distributions, including strong gradients, can also be determined. This information can change the philosophy of the experimental method—from extracting a single material mechanical property to identification of multiple material properties in

stress-strain relations from one single experiment. Thus full-field measurements by digital image correlation technique have the capability of greatly improving efficiency for constitutive parameter determination in advanced composites.

Many different identification techniques have been developed to extract constitutive parameters from a full-field displacement measurement [1]. For instance, the Virtual Field Method [2], which is based on the principle of virtual work written with a particular virtual field, can be used for identification of parameters in linear or nonlinear constitutive equations for composites [1]. Another method, Finite Element Method Updating (FEMU) method, can also be used to extract material parameters in a constitutive model. It allows the result of a numerical simulation to match the experimental field in the sense of a given norm. Based on various cost functions, such as constitutive equation gap or equilibrium gap, constitutive parameters can be identified as the minimum of the cost function by updating finite element model iteratively. The FEMU methodology is *a priori* suited for a wide range of applications, featuring complex geometrical and loading configurations [1]. In previous studies, four orthotropic planar elasticity parameters have been identified from uniaxial test of an open-hole specimen using the FEMU method. Elastic properties of monolithic ceramic were identified using a high-order polynomial displacement field in the FEMU method.

Full-field measurement methods, such as DIC, provide very densely discrete measurements of the displacement field with random error induced by the sensor noise in DIC. A reconstruction approach has to be applied to generate a continuous displacement field and strain field for material properties extraction, which induces the approximation error in the reconstruction procedure. Thus, it is essential to assess the effect of the reconstruction parameter on the uncertainties of the reconstructed displacement and strain fields. In addition, strain fields calculated by a direct finite difference approximation can amplify the random error in the displacement measurement. The error, which has been assumed to be additive and uncorrelated white noise, leads to further uncertainties in the composite material constants. It is a key issue to quantify explicitly uncertainties in the identified material constants induced by the random error in displacement measurements and the approximation error in the reconstruction procedure.

The purpose of the work is to present the use of a global finite-element-approximation method to reconstruct discrete displacement data with random measurement error, which is generated from DIC measurements for short-beam-shear (SBS) composite specimens as an illustration. The statistics of the measurement error in the displacement field due to the sensor noise in DIC have been evaluated based on the current experimental configuration. The effects of the measurement error and the reconstruction parameter on the reconstructed displacement and strain fields have been given. A squared-difference cost function has been constructed to evaluate the agreement between the DIC-reconstructed strains and the numerical calculated strains generated using FEM analysis. Multiple material constants to characterize linear axial normal and nonlinear in-plane shear stress-strain relationships have been extracted simultaneously through minimization of the cost function by a least-squares regression method. The uncertainties of the extracted material constants induced by the measurement error in displacement field and the approximation error in the reconstruction procedure have been derived explicitly.

## 2 EXPERIMENTS

In order to investigate the effects of the noise of the sensor in DIC and reconstruction parameter on the displacement and strain field assessment and present a uncertainty analysis of the extracted multiple material constants, a customized short-beam-shear test for a prismatic composite specimen at room-temperature ambient conditions was performed as an illustration [3, 4]. The coupon is machined from a 6.4 mm thick unidirectional IM7/8552 tape panel which had been cured at 350°F using the manufacturer's specification for cure time. A schematic of the short-beam specimen configuration and experimental setup with loading configuration (3-point) is shown in Figure 1. Loading was applied in the 1-3 (interlaminar) principal material plane, which permitted characterization of multiple constitutive relations along 1-3 principal material directions. The test, performed with a servo-hydraulic load frame, involved loading the specimen until failure at a fixed axial displacement rate of 1.27 mm/min crosshead displacement rate.

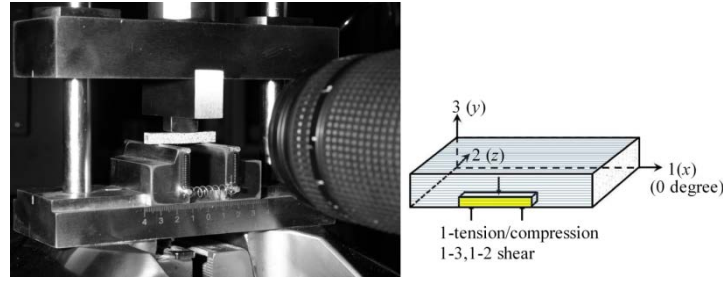


Figure 1: The short-beam shear experimental arrangement combined with DIC full-field displacement measurement to determine multiple stress-strain properties of composites from a single experiment.

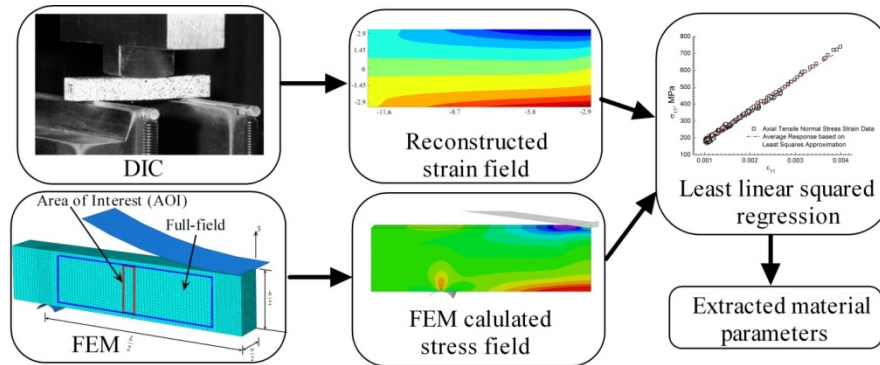


Figure 2: Schematic flowchart for the material constant identification procedure using a short-beam shear experiment combined with a general FEMU method. An ordinary least squares regression optimization technique was applied.

During testing, the surface displacement field was recorded using a DIC full-field measurement technique, which is based on the analysis of stereo images of the coupon surface which contained random speckles. While the specimen was subject to loading, a sequence of images was acquired at 1 s interval using a stereo camera system. The stereo images were obtained with a 16-mega pixel camera system. The discrete and noisy displacement field was determined iteratively from the minimization of the grey-value squared difference - summed over all pixels in a small subset area throughout the acquired stereo image sequence using software VIC-3D [5]. A subset size of 29 x 29 pixels was used, corresponding to approximately 0.34 mm<sup>2</sup> for in the particular experiments that were performed. For the experimental arrangement used, the resolution of the image was 0.0115 mm/pixel. Displacement data with maximum spatial resolution from the DIC analysis was obtained using 1 step-size in the horizontal and vertical directions, resulting in approximately 930385 data points in the AOI per load step (Fig 2). A total of 48 images are acquired for material constitutive constant extraction consequently.

### 3 FINITE ELEMENT MODEL UPDATING

The identification of independent material constitutive parameters can be carried out by a finite-element-model updating method, which is the most generic and intuitive method. The finite-element-model updating method is based on over-determined full-field displacement measurements and allows characterizing complex constitutive laws. The principle consists of updating material parameters in finite element models iteratively to minimize the objective function, which is assessed by the sum of the squared differences between DIC-determined and FEM-computed strains. The flowchart in Fig. 2 has been used for material characterization. A cost function  $Q$  can be expressed in terms of unweighted least-squared difference between the experimentally determined and numerically calculated strains:

$$Q(\bar{p}) = Q(\{\varepsilon(\bar{p})\}) = \sum_{i=1}^n (\{\varepsilon_i^{FEM}(\bar{p})\} - \{\varepsilon_i^{rec}\})^2 \quad (1)$$

where  $\bar{p}$  represents a set of unknown material parameters and  $n$ - the number of data used for evaluation of the squared differences.  $\varepsilon^{FEM}$  and  $\varepsilon^{rec}$  are the FEM-calculated strain components and reconstructed strain components derived from DIC measured displacement respectively.

The following constitutive model was used for specimens loaded in the 1-3 principal material plane [6]:

$$\begin{Bmatrix} \varepsilon_{11} \\ \varepsilon_{33} \\ \gamma_{13} \end{Bmatrix} = \begin{bmatrix} \frac{1}{E_{11}} & -\frac{\nu_{31}}{E_{33}} & 0 \\ -\frac{\nu_{13}}{E_{11}} & \frac{1}{E_{33}} & 0 \\ 0 & 0 & f(\tau_{13}) \end{bmatrix} \begin{Bmatrix} \sigma_{11} \\ \sigma_{33} \\ \tau_{13} \end{Bmatrix} \quad (2)$$

where nonlinear shear stress-strain relations are characterized by the Ramberg-Osgood equation with three material parameters ( $G_{13}, k_{13}, n_{13}$ )

$$\gamma_{13} = \frac{\tau_{13}}{G_{13}} + \left( \frac{\tau_{13}}{k_{13}} \right)^{n_{13}} \quad (3)$$

After substituting Eqn. (2) and (3) into the cost function, it is related to the FEM-calculated stresses  $\sigma_i^{FEM}$ , the reconstructed strains  $\varepsilon_i^{rec}$  and the set of unknown material constants  $\bar{p}$ . To minimize the cost function, its partial derivative with respect to the material parameter is set to zero.

$$\frac{\partial Q(\bar{p})}{\partial p_i} = \sum_{i=1}^n \left[ f(\sigma_i^{FEM}(\bar{p})) - \varepsilon_i^{rec} \right] \frac{\partial f(\sigma_i^{FEM}(\bar{p}))}{\partial p_i} = 0 \quad (4)$$

Data points ( $\sigma_i^{FEM}, \varepsilon_i^{rec}$ ) can be used in solving an ordinary least squares regression problem to generate the average stress-strain response. The set of material properties can be extracted from solving the least squares problem of Eqn. (4). For instance, the material properties to characterize the axial normal stress-strain behavior can be extracted through the ordinary least-squares (OLS) regression as:

$$\{\bar{p}\} = ([\sigma^{FEM}]^t [\sigma^{FEM}])^{-1} [\sigma^{FEM}]^t [\varepsilon^{rec}] \quad (5)$$

It can be seen from Eqn. (5) that the uncertainties in the extracted material constants can only be tracked to the uncertainties of the reconstructed strain field. Three material constants ( $G_{13}, k_{13}, n_{13}$ ) in the log-linear shear stress-strain constitutive relation can also be updated in the finite element model and determined using OLS regression method.

To extract the material constants, a three-dimensional finite element model was developed using ABAQUS. The model involves geometric nonlinearity, material nonlinearity, and contact interactions. Since symmetric boundary conditions are applied in the width and the length direction, only one quarter of the specimen was modeled. Multiple steps are defined in the analysis to match the load steps at which the DIC measurements were taken. Eqn. (2) and Eqn. (3) are implemented in the orthotropic elastic model using the user defined subroutine UMAT available in ABAQUS. The constitutive model for IM7/8552 unidirectional tape was assumed to obey transverse isotropy. An initial set of linear material constitutive parameters used by UMAT were obtained from the manufacturer's specification [19]. It has been shown that the identification procedure is quite robust and insensitive to the initial approximation of the material constitutive parameters due to the "geometric" stress distribution [15, 16]. The FEM-calculated stress and DIC-reconstructed strain at the nodes are used in the least-squares regression method.

## 4 UNCERTAINTY ANALYSES

### 4.1 Displacement field measurement and reconstruction

The full-field displacement measurements for deriving the strain field in the AOI are the discrete and noisy displacements given through DIC measurement at the  $N$  data points:

$$\begin{aligned} u^{DIC}(x_i, y_i) &= u^{ex}(x_i, y_i) + \delta u(x_i, y_i) \\ v^{DIC}(x_i, y_i) &= v^{ex}(x_i, y_i) + \delta v(x_i, y_i) \end{aligned} \quad (6)$$

$u^{ex}$  and  $v^{ex}$  is are the unknown exact displacement components along the  $x$  and  $y$  direction.  $\delta u$  and  $\delta v$  represent the error in the DIC measurement, which are assumed to be additive and uncorrelated Gaussian distribution. The covariance matrix of the random measurement error  $\delta u$  and  $\delta v$  are given as:

$$cov(\{\delta u\}) = cov(\{\delta v\}) = \sigma^2 [I] \quad (7)$$

where  $[I]$  is the identify matrix and  $\sigma^2$  is the variance of the assumed Gaussian error.

The procedure is intended for deriving the strain field from a set of discrete and noisy full-field displacement measurements. The full-field displacement measurements can be reconstructed using a global finite-element (FE) based approximation approach over the AOI zone [13, 14]. A global finite-element based approximation approach was chosen for the reconstruction. This approach was chosen as the basis functions have only low interactions between each other and it limits reconstruction oscillations as the precision increases [7]. The reconstruction parameter is the mesh size of the global FE based approximation method.

The displacement field can be written as:

$$\begin{aligned} u(x, y) &= [f(x, y)]\{U\} \\ v(x, y) &= [f(x, y)]\{V\} \end{aligned} \quad (8)$$

where  $[f(x, y)]$  is the elementary matrix of the shape functions evaluated at an arbitrary point.  $\{U\}$  and  $\{V\}$  are the columns of the nodal displacements along the  $x$  and  $y$  axis. Denoting  $[F]$  as the assembled matrix made up of all the matrices  $[f(x_i, y_i)]$  stacked,  $i \in [1, N]$  provides the following expressions for the reconstructed displacements:

$$\begin{aligned} \{u^{rec}\} &= [F]\{U\}_n \\ \{v^{rec}\} &= [F]\{V\}_n \end{aligned} \quad (9)$$

$\{u^{rec}\}$  and  $\{v^{rec}\}$  are the columns made up of all the values of  $u^{rec}(x_i, y_i)$  and  $v^{rec}(x_i, y_i)$ ,  $i \in [1, N]$ .  $n$  is the number of the nodes in the global FE based approximation, where  $N \gg n$ . Based on the least-squares minimization,  $\{U\}$  and  $\{V\}$  are the solutions of the following minimization:

$$\begin{aligned} \min_{\{U\}} \| [F]\{U\} - \{u^{DIC}\} \|^2 &\Leftrightarrow \min_{\{U\}} ([F]\{U\} - \{u^{DIC}\})^t ([F]\{U\} - \{u^{DIC}\}) \\ \min_{\{V\}} \| [F]\{V\} - \{v^{DIC}\} \|^2 &\Leftrightarrow \min_{\{V\}} ([F]\{V\} - \{v^{DIC}\})^t ([F]\{V\} - \{v^{DIC}\}) \end{aligned} \quad (10)$$

In order to solve the over-determined minimization problem, two linear systems can be derived, which give the nodal displacements as:

$$\begin{aligned} \{U\} &= [R]^{-1}[F]^t\{u^{DIC}\} \\ \{V\} &= [R]^{-1}[F]^t\{v^{DIC}\} \end{aligned} \quad (11)$$

The covariance matrices of  $\{U\}$  and  $\{V\}$  are determined by the covariance matrix of the experimental obtained data  $\{u^{DIC}\}$  and  $\{v^{DIC}\}$ . From Eqn. (6), (7) and (9),

$$cov(\{U\}) = cov(\{V\}) = \sigma^2[R]^{-1} \quad (12)$$

It can be seen that the error in the reconstructed displacement field depends on both the variance of the assumed Gaussian error in the DIC measurement and the regularization matrix  $[R]$ .

## 4.2 Strain field reconstruction

The strain field can be derived from  $\{u^{rec}\}$  and  $\{v^{rec}\}$  by differentiating the shape functions. Three strain-field components can be written as:

$$\begin{aligned} \{\tilde{\varepsilon}_{xx}\} &= \left\{ \frac{\partial u^{rec}}{\partial x} \right\} = [A]\{U\} \\ \{\tilde{\varepsilon}_{yy}\} &= \left\{ \frac{\partial v^{rec}}{\partial y} \right\} = [B]\{V\} \\ \{\tilde{\gamma}_{xy}\} &= \left\{ \frac{\partial u^{rec}}{\partial y} + \frac{\partial v^{rec}}{\partial x} \right\} = [A]\{V\} + [B]\{U\} \end{aligned} \quad (13)$$

where  $[A] = \left[ \frac{\partial F}{\partial x} \right]$  and  $[B] = \left[ \frac{\partial F}{\partial y} \right]$ . Only infinitesimal strains are considered. However the derived strain field is discontinuous and not appropriate for the material properties extraction procedure. Hence another continuous strain field has to be reconstructed using a similar global FE based approximation approach. The reconstructed strain component is given as:

$$\{\varepsilon^{rec}\} = [F]\{E\} \quad (14)$$

The linear reconstruction shape function allows the integration can be calculated analytically, providing matrices that are similar to the stiffness matrices in finite element analysis. The nodal strain component is obtained from the solution of the following linear system:

$$\{E\} = [K]^{-1}\{b\} \quad (15)$$

where the components of  $[K]$  and  $\{b\}$  can be calculated through integration over the AOI. For instance, the nodal normal strain component  $\{E_{xx}\}$  related matrix and vector can expressed as:

$$\begin{aligned} K_{ij} &= \int_{\Omega} F_i(x, y) F_j(x, y) d\Omega \\ b_i &= \int_{\Omega} F_i(x, y) \sum_{j=1}^n A_j U_j d\Omega \end{aligned} \quad (16)$$

It has been noted that the matrix  $[K]$  is only related to the reconstruction parameter in the global finite-element based approximation and remains the same once the mesh has been determined. The vector  $\{b\}$  depends on both the reconstructed displacement field and the mesh size in the reconstruction. Eqn. (21) can be written in the matrix form as:

$$\begin{aligned} \{E_{xx}\} &= [R^\varepsilon]^{-1} [F^\varepsilon]^t [A^\varepsilon] [R]^{-1} [F]^t \{u^{DIC}\} \\ \{E_{yy}\} &= [R^\varepsilon]^{-1} [F^\varepsilon]^t [B^\varepsilon] [R]^{-1} [F]^t \{v^{DIC}\} \\ \{\Gamma_{xy}\} &= [R^\varepsilon]^{-1} [F^\varepsilon]^t ([A^\varepsilon] [R]^{-1} [F]^t \{v^{DIC}\} + [B^\varepsilon] [R]^{-1} [F]^t \{u^{DIC}\}) \end{aligned} \quad (17)$$

where  $R_{ij}^\varepsilon = K_{ij}$ ,  $[F^\varepsilon]$ ,  $[A^\varepsilon]$  and  $[B^\varepsilon]$  are calculated based on the integration given in Eqn. (16). Thus, the continuous reconstructed strain component field  $\{\varepsilon^{rec}\}$  can be determined through Eqn. (14).

The covariance matrix of the nodal strain induced by the random error in the displacement measurement can be determined based on Eqn. (12) and (17). For instance, the covariance of the nodal normal strain component can be derived:

$$cov(\{E_{xx}\}) = \sigma^2 [R^\varepsilon]^{-1} [G^\varepsilon]^t [R]^{-1} [G^\varepsilon] [R^\varepsilon]^{-1} \quad (18)$$

where  $[G^\varepsilon] = [A^\varepsilon]^t [F^\varepsilon]$ . The off-diagonal terms are at least one order of magnitude lower than the diagonal ones in Eqn. (16) and (23). In addition, the diagonal terms of  $cov(\{E_{xx}\})$  are nearly equal. Thus the variance of the reconstructed strain field  $\{\varepsilon^{rec}\}$  can be approximated by the averaged diagonal terms of  $cov(\{\varepsilon^{rec}\})$ . The same trend has been reported in Ref [7] and [8]. Therefore the standard deviation of the reconstructed strain  $Std(\{\varepsilon^{rec}\}) = \alpha_{\{\varepsilon\}} \sigma$ . It can be seen that it is proportional to the standard deviation of the assumed Gaussian random error in the DIC measurement and the reconstruction procedure.

	$\bar{p}_1$ ( $1/E_{11}$ )	$\bar{p}_2$ ( $v_{31}/E_{33}$ )	$\bar{p}_3$ ( $1/G_{13}$ )	$\bar{p}_4$ ( $1/k_{13}$ )	$\bar{p}_5$ ( $1/n_{13}$ )
$\frac{\partial \varepsilon_{11}^{rec}}{\partial \{\bar{p}\}}$	$\sigma_{11}^{FEM}$	$-\sigma_{33}^{FEM}$	0	0	0
$\frac{\partial \varepsilon_{11}^{rec}}{\partial \{\bar{p}\}}$	$-\sigma_{33}^{FEM}$	$\sigma_{11}^{FEM}$	0	0	0
$\frac{\partial \gamma_{13}^{rec}}{\partial \{\bar{p}\}}$	0	0	$\tau_{13}^{FEM}$	$\left(\frac{\tau_{13}^{FEM}}{n_{13}}\right) \left(\frac{\tau_{13}^{FEM}}{k_{13}}\right)^{\left(\frac{1}{n_{13}}-1\right)}$	$\left(\frac{\tau_{13}^{FEM}}{k_{13}}\right)^{\frac{1}{n_{13}}} \ln\left(\frac{\tau_{13}^{FEM}}{k_{13}}\right)$

Table 1: The entrance of the sensitivity matrix  $[N]$  in the identification procedure

### 4.3 Uncertainty analysis

The global least-squares finite-element approximation reconstruction approach coupled with the FEMU is suited to trace the uncertainties of identified material constants based on the identification method. From Eqn. (5), the uncertainties of identified material constants depend only on the reconstructed strain data, which can be determined by Eqn. (18). Thus the uncertainties are governed by the mesh size in the global finite-element reconstruction and the variance of the Gaussian noise in the DIC measurement. Thus, the covariance matrix of the identified material constant can be derived from the OLS regression method as:

$$[C_{\{\bar{p}\}}] = \alpha_{\{\varepsilon\}}^2 \sigma^2 ([N]^t [N])^{-1} = \alpha_{\{\varepsilon\}}^2 \sigma^2 \left( \begin{bmatrix} \frac{\partial \varepsilon_i^{rec}}{\partial \bar{p}_j} \end{bmatrix}^t \begin{bmatrix} \frac{\partial \varepsilon_i^{rec}}{\partial \bar{p}_j} \end{bmatrix} \right)^{-1} \quad (19)$$

The sensitive matrix  $[N]$  can be evaluate through the constitutive relationship given in Eqn. (2) and (3), which has been given in Table 1. The diagonal terms give the variance for each parameter separately, and the off-diagonal terms provide the uncertainty to characterize all couplings between identified constants, which have not been taken into account in the present discussion. It has been clarified that the variance of the identified material constant is proportional to the variance of the assumed Gaussian distributed random error induced by the sensor noise in DIC measurement and related to the reconstruction parameter - which is the mesh size in the global finite-element approximation approach, denoted  $h$ .

## 5 RESULTS AND DISCUSSIONS

### 5.1 Reconstruction results

In order to verify the displacement and strain reconstruction results, a comparison of fields derived from synthetic data and the constructed fields has been made. The significance of synthetic data is that the exact displacement field and the measurement errors can be given as known parameters, allowing approximation errors due to the global reconstruction approach to be evaluated quantitatively. The synthetic data have been obtained from the same three-dimensional solid finite-element model developed in Section 3. However, the mesh was refined significantly to generate much more synthetic displacement and strain data, which was used to replace the experimental data obtained from the DIC measurements. The linear material constitutive properties used in the model to generate synthetic data were obtained from the prepreg manufacturer as an approximation.

Reconstruction was performed based on synthetic data without random noise initially. Thus, the error in the reconstructed field is only induced from the global finite-element-approximation approach. For the sake of simplicity and illustration purpose, the mesh used in the global finite-element-approximation reconstructed approach was square and a reconstruction mesh size  $h = 0.24$  mm was applied in the illustration.

To evaluate the effect of the mesh size on the reconstruction error, the normalized average displacement and strain reconstruction error is defined as:

$$\bar{\epsilon}_u = \frac{1}{M} \sum_{i=1}^M \left[ \frac{(u^{rec} - u^{syn})^2 + (v^{rec} - v^{syn})^2}{(u^{syn})^2 + (v^{syn})^2} \right]^{\frac{1}{2}}$$

$$\bar{\epsilon}_\epsilon = \frac{1}{M} \sum_{i=1}^M \left[ \frac{(\epsilon_{xx}^{rec} - \epsilon_{xx}^{syn})^2 + (\epsilon_{yy}^{rec} - \epsilon_{yy}^{syn})^2 + (\gamma_{xy}^{rec} - \gamma_{xy}^{syn})^2}{(\epsilon_{xx}^{syn})^2 + (\epsilon_{yy}^{syn})^2 + (\gamma_{xy}^{syn})^2} \right]^{\frac{1}{2}} \quad (20)$$

Where  $M$  is the total number of reconstruction points in the area used for identification of material properties. Using synthetic data, Figure 3 shows the variation of the normalized average displacement and strain reconstruction errors with the mesh size  $h$ . For the case without random error, it can be seen that the average reconstruction error induced by the reconstruction approximation decreases and saturate with decreasing mesh size. However, the normalized average strain reconstruction error is remarkably higher than the normalized average displacement reconstruction error, which suggests that constructing the cost function using reconstructed displacement field can reduce the uncertainty of the material constant induced by the reconstruction error in the identification.

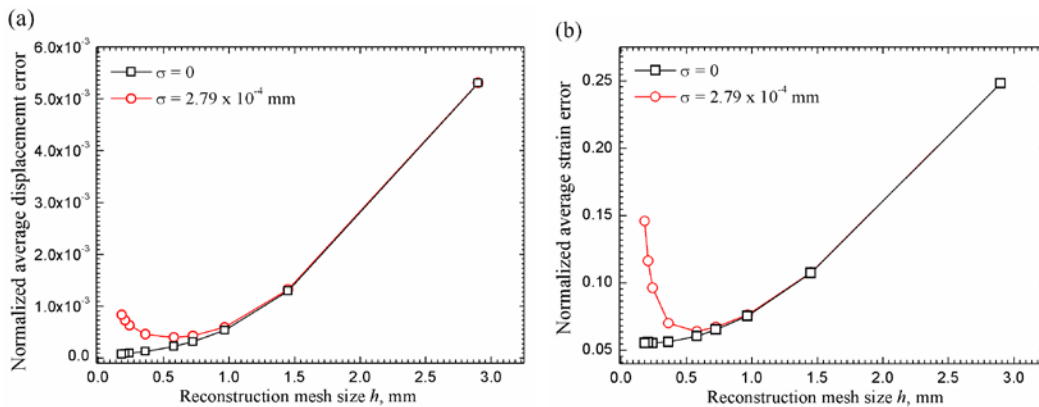


Figure 3: Variations of the normalized average error with mesh size  $h$  using synthetic data.(a) Normalized average displacement error; (b) Normalized average strain error

One objective of the work is to investigate the effect of Gaussian distributed displacement measurement error on the reconstructed displacement and strain fields, and the identification of constitutive law. In order to visualize the effects of the measurement error and the reconstruction, Gaussian distributed noise with a standard deviation of  $\sigma = 2.79 \times 10^{-4}$  mm has been added to the synthetic data, which is 10 times higher than the average confident margin  $\sigma_0 = 2.79 \times 10^{-5}$  mm, which is the average confidence margin provided by VIC-3D software for the current SBS configuration. The

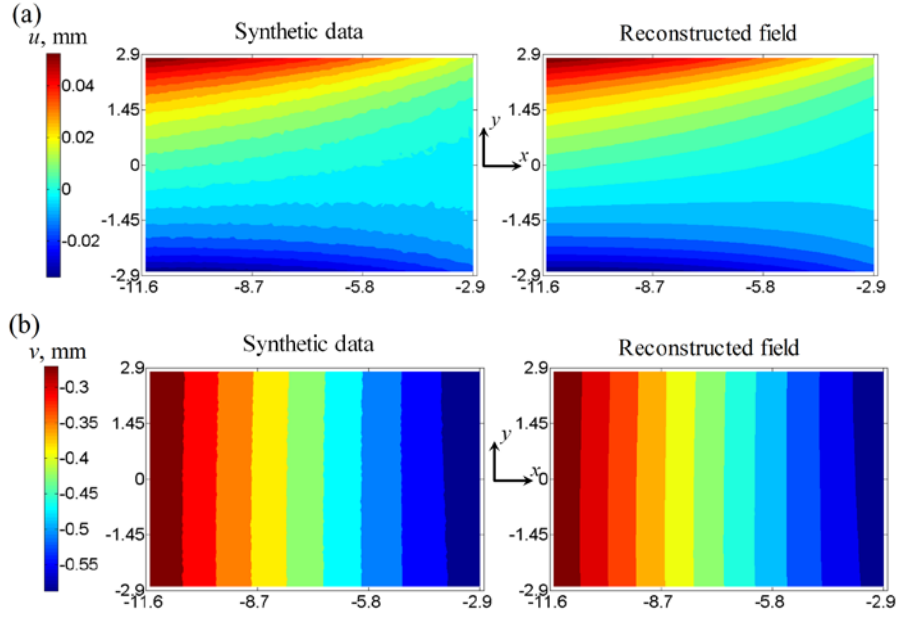


Figure 4: The displacement fields from synthetic data with measurement error and the reconstructed results. A Gaussian distributed measurement error with  $\sigma = 2.79 \times 10^{-4}$  mm is superimposed in the synthetic data with  $h = 0.32$  mm. (a) Displacement along  $x$ -axis, (b) Displacement along  $y$ -axis.

average confident margin  $\sigma$  given by VIC-3D software is used to estimate the standard deviation of the displacement measurement error before reconstruction since it provides meaningful error metric with taking into account signal-to-noise ratio of the image. Figure 4 shows displacement fields  $u$  and  $v$  from the synthetic data superimposed with the Gaussian distributed error and reconstructed fields. It is worth noting that the discrete noisy displacement fields have been reconstructed. The displacement error has been reduced significantly.

Figure 3 also shows the variation of the normalized average displacement and strain error with the reconstructed mesh size  $h$ , where the total error is attributed to the Gaussian distributed measurement error and reconstruction approximation error. It has been seen that the variations are non-monotonic since the error induced by the Gaussian distributed error increases with decreasing mesh size. Thus the optimized mesh size can be achieved with minimization of the normalized total error. It is inferred that the optimized mesh size depends both on the standard deviation of the displacement measurement error and the gradient of the displacement field. An optimized reconstruction mesh size can be obtained to tune the noise and the approximation error in the reconstruction field, which reduces the total error. It is worth noting that the strain error is also much higher than the displacement error for the case with Gaussian displacement noise. This indicates that to reduce the effects of approximation and random displacement measurement error, it is beneficial to identify material constants from the reconstructed displacement field.

## 5.2 Identification results and uncertainties

The ordinary least-squares approximation presented in Section 3 can be used to extract the orthotropic material stress-strain constants for the unidirectional SBS specimen loaded along the 1-3 principal material plane. The initial numerically-calculated stress components extracted from the AOI of the three-dimensional solid finite-element-model (Fig. 2) is combined with the reconstructed strain components. The material constitutive relationship is generated by coupling the FEM-calculated stress and DIC-reconstructed strain and updated. This iterative procedure continues until the change in the constitutive model is negligible. The convergence criteria used as the threshold to stop the iteration is that the relative value of the parameter(s) in the constitutive relationship updates less than 0.5%, and the variation of the normalized square root of the objective function in Eqn. (1) is less than 1%.



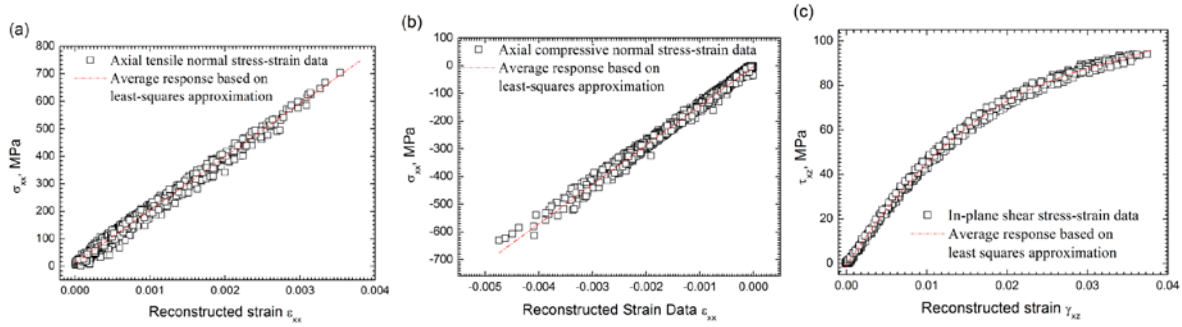


Figure 5: Typical converged result for the material constitutive relationship derived through least-squares approximation coupling of reconstructed strain and FEM-calculated stress using the data points in the AOI. (a) Axial normal tensile stress-strain data and average response; (b) Axial normal compressive stress-strain data and average response; (c) In-plane shear stress-strain data and average response.

Figure 5 shows the typical converged results for the linear least-squares regression between FEM-calculated stress and the DIC-reconstructed strain in the AOI. The reconstruction mesh size, which is determined by minimization of the average strain reconstruction error, has been adjusted for each image. The data indicates (Fig. 5) a linear relationship between axial normal stress and strain can be identified for extraction of tensile and compressive axial Young's modulus. A three-parameter Ramberg-Osgood relationship between shear stress and strain is identified as well in Fig 5(c). It is noteworthy that the average strain reconstruction error depends both on the variance of the Gaussian distributed displacement measurement error and the mesh size in the reconstruction. However the optimal mesh size is unknown since the gradients of the displacement and strain field are not known. In order to determine an appropriate reconstruction mesh size, the linear material constitutive properties were assumed with materials constants provided by the prepreg manufacturer, and a numerical FEM simulation was performed to generate synthetic strain data. The synthetic field is an approximation to experimental obtained strain field with underestimated displacement and strain gradients due to material linearity. The appropriate reconstruction mesh size can be estimated by minimization of the average strain reconstruction error defined by Eqn. (20). The estimated optimal reconstruction mesh size for each image can be evaluated and used in the experimental strain field reconstruction. With the standard deviation of the displacement measurement error  $\sigma_0 = 2.79 \times 10^{-5}$  mm, appropriate reconstruction mesh sizes have been determined for each image used in the material constants extraction.

Material constants	AOI			Full Field		
	Mean	Standard Deviation (SD)	Coefficient of Variance (COV)	Mean	Standard Deviation (SD)	Coefficient of Variance (COV)
$1/E_{11T}$ , 1/GPa	1/187.9	1/(187.9×11.1)	9.0%	1/193.5	1/(193.5×29.9)	3.35%
$1/E_{11C}$ , 1/GPa	1/142.3	1/(142.3×13.2)	7.58%	1/141.3	1/(141.3×39.1)	2.56%
$\nu_{31}/E_{33}$	0.022/8890	(0.0218×0.014)/8890	13.6%	0.019/8788	(0.0189×0.047)/8788	4.68%
$1/G_{13}$ , 1/MPa	1/4563.1	1/(4563.1×112.3)	0.89%	1/4348.5	1/(4348.5×234)	0.43%
$1/k_{13}$ , 1/MPa	1/221.25	1/(221.25×49.8)	2.01%	1/218.79	1/(218.79×99)	1.01%
$n_{13}$	1/4.32	1/(4.32×42)	2.38%	1/4.47	1/(4.47×84.8)	1.18%

Table 2: The standard uncertainty of each identified material constitutive properties for the unidirectional SBS specimens loaded in 1-3 principal material plane

The converged expectation, standard deviation and the coefficient of variation (COV) of the identified material constants based on the DIC-reconstructed strain and the FEM-calculated stress in the AOI and full-field area have been listed in Table 2. The results demonstrate that the COV for the

axial tensile, compressive Young's modulus and Poisson ratio related parameter are higher than the parameters used to characterize the in-plane shear Ramberg-Osgood relationship due to higher in-plane shear strain amplitude.

The results also indicate that the material constants identified from the smaller AOI are consistent with those extracted from the full-field area and the maximum deviation is no more than 5%. It is interesting to be noted that the COV determined from the full-field is smaller than that determined from the AOI. The reason is that the variance of the identified constant depends on the sensitive matrix  $N$ , which is related to the stress data. Thus the variance of the identified constant is inversely proportional to the summation of squared deviation to mean of the stress data points. The number of the stress data points in the full-field is much more than the number of the stress data points in the AOI, which induces smaller variance of the identified material constant and the COV as well. The comparison suggests that the expectation of the material constant can be determined from smaller AOI [3, 4], but the variance of the material constant is higher than that determined from the larger full-field area.

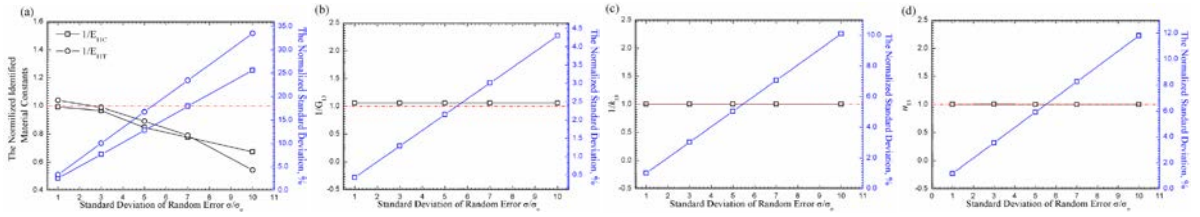


Figure 6: The variations of the identified material constant and the standard deviation with the standard deviation of the Gaussian distributed measurement error, in which the identified constant and the standard deviation have been normalized by the nominal value. (a)  $1/E_{11C}$  and  $1/E_{11T}$ ; (b)  $1/G_{13}$ ; (c) The value of  $1/k_{13}$  in Ramberg-Osgood relationship; (d) The value of  $n_{13}$  in Ramberg-Osgood relationship.

Uncertainties of identified material properties are governed by the variance of the displacement measurement error and the reconstruction mesh size used in the global finite-element based approximation approach. The variance of an identified material constant is proportional to the variance of the displacement measurement error as the optimal reconstruction mesh size remains the same. This is verified in Fig. 6 using synthetic data, in which the identified material constant has been normalized by the nominal value. A standard deviation of  $\sigma$  has been added to the synthetic data to characterize the displacement measurement error. The right axis represents the normalized standard deviation of the identified material constant, which increases linearly with the standard deviation of the displacement measurement error. It is noteworthy that material constants used to characterize in-plane nonlinear shear stress-strain behavior show strong robustness to the displacement measurement error and can be readily identified. Very good agreement between the identified material constants and the nominal values was achieved if the standard deviation of the measurement error is less than  $10\sigma_0$  (Figs. 6b, c and d). However, the axial Young's modulus extracted from the AOI in the SBS test is sensitive to the standard deviation of the displacement measurement error—a reliable material constant cannot be identified with the standard deviation of the measurement error larger than  $3\sigma_0$ . This occurs because of increased sensitivity to random measurement error when the reconstructed normal strain component  $\varepsilon_{xx}^{rec}$  is much smaller than the reconstructed shear strain component  $\gamma_{xy}^{rec}$  in the AOI of the SBS test.

Figure 7 shows the variations of the normalized identified material constant and its standard deviation with the reconstruction mesh size  $h$  as the standard deviation of the random error  $\sigma_0 = 2.79 \times 10^{-5}$  mm is superimposed in the synthetic data. The results indicate that the identified material constants are quite sensitive to the reconstruction mesh size. With increasing mesh size, all extracted material constants deviate significantly from the given nominal values. However the variance of the identified material constant *decreases* with increasing reconstruction mesh size; this is related to dependence on the standard deviation of the reconstructed strain, which decreases with increasing mesh size. It has been pointed out that no parameter can be extracted reliably if an inappropriate

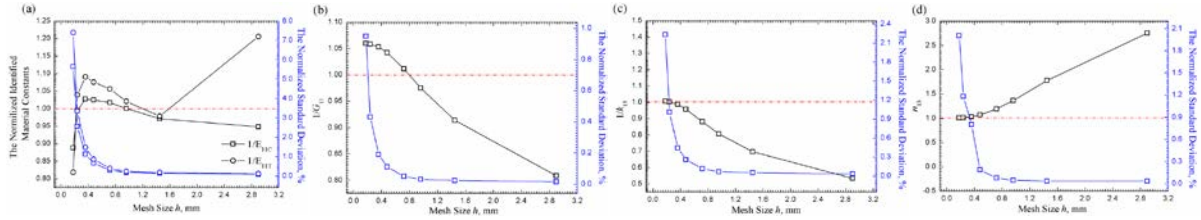


Figure 7: The variations of the identified material constant and its standard deviation with the reconstruction mesh size, in which the identified constant and the standard deviation have been normalized by the nominal value. (a)  $1/E_{11C}$  and  $1/E_{11T}$ ; (b)  $1/G_{13}$ ; (c) The value of  $1/k_{13}$  in Ramberg-Osgood relationship; (d) The value of  $n_{13}$  in Ramberg-Osgood relationship.

mesh size is used for reconstruction. Thus an estimation of an appropriate reconstruction parameter, based on minimization of average strain reconstruction error using synthetic data or other complementary prior information is necessary for improving reliability of material constant identification procedures.

## 5 CONCLUSIONS

The uncertainty analysis of displacement measurement and strain assessment due to intrinsic measurement error in digital image correlation (DIC) technique and the reconstruction approximation method is illustrated through a customized short-shear-beam experiment in this work. The uncertainty of the extracted material constants has been derived. As an illustration, multiple orthotropic material constants in the constitutive relation for a unidirectional composite specimen has been extracted simultaneously based on ordinary linear least-squares regression and FEMU method using coupled FEM-calculated stress and DIC-reconstructed strain. The uncertainty including the expectation and the standard deviation of the identified material constant has been presented. The uncertainty of the constant determined from the smaller AOI and the full-field area has been compared. The effect of the number of the image used in the identification on the uncertainty of the constant has been investigated. Using the synthetic data, the effects of the intrinsic measurement error and the reconstruction parameter on the uncertainty of identified material constant have been discussed.

The analysis demonstrated that the DIC measured discrete and noisy displacement has been reconstructed through a global finite-element based approximation approach and the measurement error has been reduced significantly. The normalized average displacement reconstruction error is much smaller than the normalized average strain reconstruction error - suggesting that using a reconstructed displacement field in the identification is beneficial to reduce the reconstruction error effect on material constant extraction. The average strain reconstruction error induced by the Gaussian measurement error increases with decreasing reconstruction mesh size; and the approximation error due to numerical reconstruction approximation method decreases with decreasing mesh size. Thus, an optimized reconstruction mesh size exists and has been determined by tuning the Gaussian distributed measurement error and the approximation error to minimize the average strain reconstruction error. The studies demonstrate that with decreasing the variance of the measurement error, the variation of the optimized reconstruction mesh size with increasing the strain field gradient is insignificant-suggesting that one constant reconstruction mesh size can be applied for a series of images with increasing strain field gradients during loading.

The uncertainty in the identified material constant, which can be tracked to the uncertainty of displacement field, is governed by the variance of the displacement measurement error and the reconstruction mesh size. An appropriate reconstruction mesh size  $h = 0.24$  mm has been estimated by minimization of the average reconstruction strain error using synthetic data and five material constants were identified using the appropriate reconstruction mesh size as an illustration. The results show that the material constants extracted from the smaller AOI area are consistent with those extracted from the full-field area, but the standard deviation is higher. The effect of the number of images used in the identification on the uncertainty of the material constant has been investigated. The result shows the identified expectation of the material constant converges after 5 images and the COV decreases with increasing the number of the images. The investigation indicates that there exist an area of interest and

the least number of images, that the reliable expectation of the material constant can be identified from it. But much more data points used in the identification procedure lead to smaller standard deviation and COV.

The effects of the variance of the displacement measurement error and the reconstruction mesh size on the uncertainty of extracted material constant have been studied using synthetic data. The analysis indicates that the material constants used to characterize the in-plane shear stress-strain behavior show strong robustness to the Gaussian displacement measurement error. However, the identified parameters to characterize axial normal stress-strain behavior was more sensitive to the measurement error and a reliable material constant could not be identified with increasing the standard deviation of displacement measurement error. Another key finding was that the reconstruction mesh size in the global finite-element based approximation approach is critical for reliable material constants identification. As the reconstruction mesh size deviates from an appropriate value, no material constant can be extracted from the linear least-square regression procedure between FEM calculated-stress and DIC-reconstructed strain reliably.

### ACKNOWLEDGEMENTS

This work is sponsored by the National Natural Science Foundation of China under Grant No. (11472043). Dr. L. Liu is supported under the Program for New Century Excellent Talents at Chinese Universities and the 111 Project (B16003). This support is gratefully acknowledged.

### REFERENCES

- [1] S. Avril, M. Bonnet, Bretelle, A.S., M. Grédiac, F. Hild, P. Ienny *et al.* Overview of identification methods of mechanical parameters based on full-field measurements. *Exp. Mech.* 2008; **48** (4), pp. 381–402. doi:10.1007/s11340-008-9148-y.
- [2] F. Pierron and M. Grédiac, *The Virtual Fields Method*, Springer-Verlag, New York publishers, 2012. <http://dx.doi.org/10.1007/978-1-4614-1824-5>.
- [3] A. Makeev, Y. He, P. Carpentier and B. Shonkwiler. A Method for Measurement of Multiple Constitutive Properties for Composite Materials. *Compos Part A Appl Sci Manuf* 2012; **43** (12) pp. 2199-2210.
- [4] Makeev A, He Y, Schreier H. Short-Beam Shear Method for Assessment of Stress-Strain Curves for Fiber-Reinforced Polymer-Matrix Composite Materials, *Strain* 2013; 49, 440-450.
- [5] M.A. Sutton. Digital Image Correlation for Shape and Deformation Measurements; In: Sharpe WN, Editor. *Springer Handbook of Experimental Solid Mechanics*, Part C. 2008; New York: Springer, pp. 565-600.
- [6] He TR, Liu L, Makeev A, Shonkwiler B, Characterization of stress–strain behavior of composites using digital image correlation and finite element analysis, *Composite Structures* 2016; **140**, pp. 84-93. DOI:10.1016/j.compstruct.2015.12.018.
- [7] S. Avril, P. Feissel, F. Pierron, P. Villon. Comparison of two approaches for differentiating full-field data in solid mechanics, *Meas. Sci. Technol* 2010; **21**:015703. doi:10.1088/0957-0233/21/1/015703.
- [8] R. Gras, H. Leclerc, F. Hild, S. Roux and J. Schneider. Identification of a set of macroscopic elastic parameters in a 3D woven composite: Uncertainty analysis and regularization, *Int J Solids Struct* 2015; **55** pp. 2-16. DOI:10.1016/j.ijsolstr.2013.12.023.